Z. Angew. Math. Phys. (2023) 74:203
© 2023 The Author(s)
0044-2275/23/050001-18
published online September 27, 2023
https://doi.org/10.1007/s00033-023-02104-8

Zeitschrift für angewandte Mathematik und Physik ZAMP

The 3-wave resonant interaction model: spectra and instabilities of plane waves

Marzia Romano, Sara Lombardo and Matteo Sommacal

Abstract. The three wave resonant interaction model (3WRI) is a non-dispersive system with quadratic coupling between the components that finds application in many areas, including nonlinear optics, fluids and plasma physics. Using its integrability, and in particular its Lax Pair representation, we carry out the linear stability analysis of the plane wave solutions interacting under resonant conditions when they are perturbed via localised perturbations. A topological classification of the so-called *stability spectra* is provided with respect to the physical parameters appearing both in the system itself and in its plane wave solution. Alongside the stability spectra, we compute the corresponding gain function, from which we deduce that this system is linearly unstable for any generic choice of the physical parameters. In addition to stability spectra of the same kind observed in the system of two coupled nonlinear Schrödinger equations, whose non-vanishing gain functions detect the occurrence of the modulational instability, the stability spectra of the 3WRI system possess new topological components, whose associated gain functions are different from those characterising the modulational instability. By drawing on a recent link between modulational instability and the occurrence of rogue waves, we speculate that linear instability of baseband-type can be a necessary condition for the onset of rogue wave types in the 3WRI system, thus providing a tool to predict the subsequent nonlinear evolution of the perturbation.

Mathematics Subject Classification. 37K10, 35B35, 35C08, 35Q35, 35Q51, 76B15, 14H70.

1. Introduction

The three wave resonant interaction (3WRI) system is a well known universal model which describes the non-dispersive propagation of waves in weakly nonlinear media [1,2]. Despite its dispersionless nature, it possesses solitons (see, e.g., [3–6] and references therein), which occur as result of the balance between nonlinearity and the energy flow due to the mismatch of the velocities of the three interacting waves (see, e.g., [1,7,8]), and it is not due to the balance between nonlinearity and dispersion as it happens for the 'traditional' solitons [9]. Such solitons are ubiquitous in many nonlinear systems of physical interest (e.g. in nonlinear optics [10]) and they have been observed experimentally in stimulated Raman scattering [11], in Brillouin finger ring laser [12] and in quadratic optical media [13]. Among its soliton solutions, rational and semi-rational solutions [14–17] have enjoyed renewed interest as they can be used to model rogue wave-type phenomena [18,19], recently observed in oceans [20], in optics [21], in the atmosphere [22], in Bose-Einstein condensates [23], and in capillary-waves [24]. They were also observed in laboratory experiments with superfluid helium [25] and generated in water tanks [26].
In dispersive systems, modulational instability (MI) has been proposed as a possible cause of the onset of rogue waves [27,28]; however, not all kinds of MIs have been considered, but only the so-called *baseband* MI [27,28], that is, a fundamental feature of nonlinear dispersive systems for which a periodic perturbation on an unstable plane wave or continuous wave background (CW) grows when the perturbation frequency is around zero (zero not included) (see, for instance, [29]). In [14,17], novel families of rational and semi-rational solutions on non-vanishing background of the integrable 3WRI system, which is instead non-dispersive, have been obtained via Darboux Dressing transformations (see, e.g., [30,31]), and they have contributed to our understanding of extreme phenomena in multi-component resonant processes.

In this work, we carry out the linear stability analysis of plane wave solutions of the 3WRI model (1), motivated by the fact that this resonant process is observed in different physical contexts such as in plasma wave interactions [32,33], in nonlinear dielectric media [34], in planetary wave interactions [35], in shear flows [36] and internal waves [37]. The non-dispersive nature of the 3WRI system makes the linear stability analysis of its solutions more intriguing. Indeed, we expect the mechanism leading to the linear instability in the 3WRI system to differ from the one associated with MI in dispersive nonlinear systems, the latter being due to the interplay between dispersion and a weak nonlinearity [38]. In particular, in dispersive multi-component systems, the coupling among the components can suppress or enhance the MI of the single component [39–41] and the dispersion plays a key-role in the occurrence of MI. For instance, it has been shown that two coupled sine-Gordon equations in the non-dispersive regime are stable with respect to MI [39]. The 3WRI system admits also dispersive shock waves [42], similar to those admitted by well known dispersive systems such as the nonlinear Schrödinger (NLS) and the Korteweg-de Vries (KdV) equation.

Despite the relevance of the 3WRI system, the linear stability analysis of its plane wave solutions has not received much attention in the literature, to the best of our knowledge. This is possibly due to algebraic difficulties in dealing with a multi-component system and solutions with nonzero boundary conditions.

In the paper, we follow [43] and adopt the approach presented in [44,45] exploiting the integrability of the system, in particular its Lax Pair formulation, to study the linear stability of its plane waves solution and classify the so-called *stability spectra* and associated gain functions. We provide a complete topological classification in the physical parameters space. Moreover, we observe that all topologies of the stability spectra of a system of two coupled nonlinear Schrödinger equations (CNLS) detailed in [44,46], as well as those of a long wave-short wave interaction system (YON) detailed in [45], are also present for the 3WRI system. Indeed, there exist open curves (branches) associated with an MI-baseband-type instability and closed curves (loops) associated with an MI-passband-type instability. However, there exist new topological features (twisted loops) in the stability spectra of the 3WRI model which do not exist for the CNLS system. They are associated with an isolated real point of the stability spectrum and, at this point, the solutions are always linearly unstable; on the contrary, the CNLS system is linearly stable for any real values of the spectral parameter outside the gaps [44,46]. Moreover, the gain function associated with these twisted loops is neither baseband-type nor passband-type, being nonzero in the whole neighbourhood of the zero wave number. Like in the CNLS case, also for the 3WRI system, we show that for a generic choice of physical parameters, the plane waves solutions are linearly unstable.

In Sect. 2, we recall the Lax pair formulation of the 3WRI model and its plane wave solution. Here, we briefly describe also the relation between the linearised equation and the squared eigenfunctions, following [44], and we introduce the concept of *stability spectrum* associated with the plane wave solution. In Sect. 3, we identify regions in the parameters space associated with different topologies of the stability spectrum and we construct the corresponding gain functions. We deduce that the plane wave solution of the 3WRI system is linearly unstable for any generic choice of the physical parameters. In the Conclusions, we summarise our results, and in particular we highlight the link between instabilities of baseband-type and the occurrence of rogue waves phenomena, proving a spectral characterisation of rogue waves type solutions, already known in the literature.

2. Stability spectra associated with the plane wave solutions

The propagation in $1 + 1$ dimensions of three resonating waves is modelled by the following system of three coupled partial differential equations (PDEs):

$$\begin{cases} u_{1t} + c_1 u_{1x} = s_1 c_2\, u_2^* u_3^*, \\ u_{2t} + c_2 u_{2x} = s_2 c_1\, u_1^* u_3^*, \\ u_{3t} = s_3 (c_1 - c_2) u_1^* u_2^*, \end{cases} \tag{1}$$

where the asterisk denotes the complex conjugate, $u_j = u_j(x,t)$ are complex valued functions of space x and time t, s_j are signs such that $s_j^2 = 1$ for $j = 1, 2$, and $c_1 \neq c_2$ are the nonzero *velocities* associated to u_1 and u_2, respectively. Indeed, without loss of generality, we have set the velocity associated with u_3 to zero, that is equivalent to choosing a reference frame co-moving with the solution u_3. The ordering of the velocities is otherwise generic at this stage. Hereinafter, subscripted variables stand for partial differentiation with respect to x or t. It is worth highlighting that (1) might look different from the one usually given in the literature (see e.g. [3] and [42]), however it contains all the possible three waves resonant interaction systems, irrespectively of the choice of signs and ordering of the velocities. This allows us to study a single Lax Pair (see (7)), instead of dealing with at least three different Lax Pairs (e.g. [3], [42]) depending on the choice of the ordering of the velocities, this being advantageous from the point of view of the classification of the stability properties of the plane waves solutions.

System (1) models the interaction of three resonating waves and, as such, it has been the subject of extensive investigation (see, for instance, [3]). It can be derived via multiscale analysis of a large class of nonlinear wave equations with weak dispersion and nonlinearity (see, for instance, [4]) and therefore it represents a universal model able to capture the lowest order corrections, due to nonlinear effects, to linear propagation. We have already pointed out that, contrary to other integrable nonlinear wave equations such as the nonlinear Schrödinger equation, the Korteweg-de Vries equation or the sine-Gordon equation, this system has no (linear) dispersion. The second peculiar characteristic is that no self-interaction occurs, namely, the forcing of each wave (i.e. the non-homogeneous term in the propagation Eq. (1)) is just the product of the (complex conjugated) amplitudes of the other two waves.

The plane wave solutions of (1) can be written as

$$u_j = a_j e^{i(\eta_j t - \nu_j x)}, \quad j = 1, 2, 3, \tag{2}$$

with a_j constant amplitudes, η_j frequencies and ν_j wave numbers. Frequencies and wave numbers are related one another via the resonant conditions

$$\eta_1 + \eta_2 + \eta_3 = 0, \quad \nu_1 + \nu_2 + \nu_3 = 0. \tag{3}$$

Thus, the solution u_3 reads

$$u_3 = a_3 e^{-i((\eta_1+\eta_2)t - (\nu_1+\nu_2)x)}, \quad a_3 = i s_3 a_1 a_2 \frac{c_1 - c_2}{\eta_1 + \eta_2}, \quad a_1, a_2 \in \mathbb{R}, \tag{4}$$

and the nonlinear dispersion relations are

$$\nu_1 = \frac{\eta_1}{c_1} + s_1 s_3 a_2^2 \frac{c_2(c_1 - c_2)}{c_1(\eta_1 + \eta_2)}, \quad \nu_2 = \frac{\eta_2}{c_2} + s_2 s_3 a_1^2 \frac{c_1(c_1 - c_2)}{c_2(\eta_1 + \eta_2)}. \tag{5}$$

System (1) is integrable, as it admits a Lax Pair (e.g., see, [3]) namely, it can be written as the compatibility condition of two linear differential equations for an unknown auxiliary matrix-valued function ψ:

$$\psi_x = X\psi, \qquad \psi_t = T\psi, \tag{6}$$

where X and T are matrix-valued functions depending on $u(x,t)$ and on a complex variable κ, called spectral parameter, as follows:

$$X = -i\kappa C + U, \quad T = i\kappa D + V. \tag{7}$$

Here

$$C = \begin{pmatrix} 0 & 0 & 0 \\ 0 & c_2 & 0 \\ 0 & 0 & c_1 \end{pmatrix}, \quad D = \begin{pmatrix} 0 & 0 & 0 \\ 0 & c_1 c_2 & 0 \\ 0 & 0 & c_1 c_2 \end{pmatrix} \tag{8}$$

$$U = \begin{pmatrix} 0 & s_1 u_1 & -s_1 s_2 s_3 u_2^* \\ s_1 s_2 s_3 u_1^* & 0 & s_3 u_3 \\ s_2 u_2 & s_1 s_2 s_3 u_3^* & 0 \end{pmatrix}, \quad V = \begin{pmatrix} 0 & -s_1 c_1 u_1 & s_1 s_2 s_3 c_2 u_2^* \\ -s_1 s_2 s_3 c_1 u_1^* & 0 & 0 \\ -s_2 c_2 u_2 & 0 & 0 \end{pmatrix}. \tag{9}$$

Note that, U and V are related as follows:

$$V = [B, [U, D]], \tag{10}$$

where the notation $[M_1, M_2]$ stands for the commutator $M_1 M_2 - M_2 M_1$ and

$$B = \begin{pmatrix} 0 & 0 & 0 \\ 0 & \frac{1}{c_2} & 0 \\ 0 & 0 & \frac{1}{c_1} \end{pmatrix}. \tag{11}$$

In this setup, for all $\kappa \in \mathbb{C}$, Eq. (1) is retrieved by imposing the compatibility condition $\psi_{xt} = \psi_{tx}$ for system (6):

$$X_t - T_x + [X, T] = 0. \tag{12}$$

A perturbation of $u_j(x,t)$ in the form $u_j + \delta u_j$ corresponds to a perturbation of X and T in the form $X + \delta X$ and $T + \delta T$ where, $\delta X = \delta X(x,t)$ and $\delta T = \delta T(x,t)$ are solutions of the linearised equation

$$(\delta X)_t - (\delta T)_x + [\delta X, T] + [X, \delta T] = 0. \tag{13}$$

Equation (13) is the evolution equation for the perturbation δU of the matrix U, that is

$$\delta U_t - [B, [\delta U_x, D]] + i\kappa[\delta U, D] - i\kappa[C, [B, [\delta U, D]]] + [\delta U, [B, [U, D]]] + [U, [B, [\delta U, D]]] = 0. \tag{14}$$

If δU is a localised perturbation, then, as proven in [44], a solution of the linearised Eq. (14) reads

$$F = i\,[C, \Psi]\,, \tag{15}$$

with

$$\Psi = \psi M \psi^{-1}, \tag{16}$$

where $M = M(\kappa)$ is an arbitrary, nonzero constant matrix. The matrix Ψ, which is essentially a *squared eigenfuction* in the spirit of [47], for any given arbitrary M, satisfies the linear ordinary differential equations (ODEs):

$$\Psi_x = [X, \Psi], \quad \Psi_t = [T, \Psi], \tag{17}$$

which are compatible with one another because of (12).
The solution F plays the same role as the exponential solution of linear equations with constant coefficients; namely, by varying κ, it provides the set of "Fourier-like" modes of the linear PDE (13). As a consequence, any sum and/or integral of F over the spectral parameter κ is a solution δU of the linearised Eq. (13). As in [44], here we assume that the perturbation δU has the integral representation

$$\delta U(x,t) = \int d\kappa\, F(x,t,\kappa). \tag{18}$$

In order to explicitly compute F, we need first to compute the solution of the Lax Eq. (6). At this stage, it is convenient to set

$$q = \eta_1 = \eta_2\,, \quad q \neq 0; \tag{19}$$

this can be done without loss of generality[1]. In this setup, the fundamental matrix solution of the Lax pair reads

$$\psi = Re^{i(x\,W - t\,Z)}, \tag{20}$$

where the matrix $R(x,t)$ is given by

$$R = e^{-\frac{i}{2}(\nu_1-\nu_2)x\mathbf{I}} e^{-i(qt-\nu_1 x)\Sigma_+} e^{i(qt-\nu_2 x)\Sigma_-}, \tag{21}$$

with $\mathbf{I}$ the 3×3 identity matrix and

$$\Sigma_+ = \begin{pmatrix} 0 & 0 & 0 \\ 0 & 1 & 0 \\ 0 & 0 & 0 \end{pmatrix}, \quad \Sigma_- = \begin{pmatrix} 0 & 0 & 0 \\ 0 & 0 & 0 \\ 0 & 0 & 1 \end{pmatrix}, \quad [\Sigma_+, \Sigma_-] = \mathbf{0}, \tag{22}$$

and where $W = W(\kappa)$ and $Z = Z(\kappa)$ are two x, t-independent matrices

$$W = 2c_1c_2q \begin{pmatrix} 0 & -is_1a_1 & is_1s_2s_3a_2 \\ -is_1s_2s_3a_1 & -\kappa c_2 - \nu_1 & -is_3a_3 \\ -is_2a_2 & -is_1s_2s_3a_3^* & -\kappa c_1 + \nu_2 \end{pmatrix}, \tag{23}$$

and

$$Z = \begin{pmatrix} 0 & -is_1c_1a_1 & is_1s_2s_3c_2a_2 \\ -is_1s_2s_3c_1a_1 & -\kappa c_1c_2 - q & 0 \\ -is_2c_2a_2 & 0 & -\kappa c_1c_2 + q \end{pmatrix}, \tag{24}$$

with the property $[W, Z] = 0$, so that $W(\kappa)$ and $Z(\kappa)$ can be diagonalised by the same matrix $G(\kappa)$, namely

$$W(\kappa) = G(\kappa)W_D(\kappa)G^{-1}(\kappa), \quad W_D = \mathrm{diag}\{w_1,\, w_2,\, w_3\}, \tag{25}$$

$$Z(\kappa) = G(\kappa)Z_D(\kappa)G^{-1}(\kappa), \quad Z_D = \mathrm{diag}\{z_1,\, z_2,\, z_3\}. \tag{26}$$

In terms of W, Z, R and M, the solution F of the linearised (14) reads

$$F(x,t,\kappa) = R(x,t)\left[\Sigma,\, e^{i(xW(\kappa)-tZ(\kappa))}M(\kappa)e^{-i(xW(\kappa)-tZ(\kappa))}\right]R^{-1}(x,t) \tag{27}$$

for each value of κ. Then, as shown in [46], in order to make (27) explicit, we write $M(\kappa)$ as a linear combination of the nine matrices

$$V^{(jm)}(\kappa) = G(\kappa)B^{(jm)}G^{-1}(\kappa), \tag{28}$$

with

$$B^{(jm)}_{kn} = \delta_{jk}\delta_{mn}, \tag{29}$$

where δ_{jk} is the Kronecker delta ($\delta_{jk} = 1$ if $j = k$ and $\delta_{jk} = 0$ otherwise), in the form:

$$M(\kappa) = \sum_{j,m=1}^{3} \mu_{jm}(\kappa)V^{(jm)}(\kappa), \tag{30}$$

where μ_{jm} are (arbitrary) scalar functions. Plugging this decomposition into (27), we obtain the following representation of F

$$F(x,t,\kappa) = R(x,t)\sum_{j,m=1}^{3} \mu_{jm}(\kappa)e^{i[(x(w_j-w_m)-t(z_j-z_m)]}F^{(jm)}(\kappa)R^{-1}(x,t), \tag{31}$$

[1] Anticipating the concept of stability spectrum which will be formally introduced at the end of this section, one can prove that the sum $\eta_1 + \eta_2$ corresponds to the scale factor which magnifies or shrinks the spectrum, whereas the difference $\eta_1 - \eta_2$ corresponds to the length of rigid translation of the spectrum along the real axis.

where $w_j = w_j(\kappa)$ and $z_j = z_j(\kappa)$, $j = 1, 2, 3$, are the eigenvalues of W and Z, respectively, and they are assumed to be simple, for a generic value of κ, and where $F^{(jm)}(\kappa)$ are the x, t-independent matrices defined as

$$F^{(jm)}(\kappa) = \left[\Sigma,\, V^{(jm)}(\kappa)\right]. \tag{32}$$

Requiring the solution to be localised in the variable x implies (see [44]) the necessary condition that the functions $\mu_{jm}(\kappa)$ be vanishing for $j = m$, $\mu_{jj} = 0$, $j = 1, 2, 3$.
Hereafter, it is convenient to introduce the following re-scaled wave amplitudes α_j and the re-scaled spectral parameter λ

$$\alpha_1 = \frac{a_1^2}{q^2}, \quad \alpha_2 = \frac{a_2^2}{q^2}, \quad \lambda = c_1\, c_2\, \frac{\kappa}{q}, \tag{33}$$

along with a re-scaling of w- and z-roots, respectively, as $w \mapsto q^2\, w$ and $z \mapsto q\, z$, and setting $q = 1$ with effect of removing the dependence on q from the roots of the characteristic polynomials of W and Z. Note that we are assuming here both c_1 and c_2 different from zero; the cases where at least one of the velocities is zero is a degenerate case (see [48] for details). Moreover, let p_1, p_2 and p_3 be real parameters defined as

$$p_1 = \frac{c_1^2 s_1 \alpha_1 + c_2^2 s_2 \alpha_2}{s_1 s_2 s_3}, \quad p_2 = \frac{c_1^2 s_1 \alpha_1 - c_2^2 s_2 \alpha_2}{s_1 s_2 s_3}, \quad p_3 = \frac{c_1 - c_2}{c_1 + c_2}, \tag{34}$$

where s_j, c_1 and c_2 are as in (1), entailing $p_3 \neq 0, \pm 1$. In the following, we will assume $c_1 + c_2 \neq 0$, and postpone the study of the counter-propagating case $p_3 \to \infty$ to future investigation. In the new parameters, the characteristic polynomial $P_W(w; \lambda)$ of W reads

$$\begin{aligned} &P_W(w;\lambda) = \\ &w^3 + (2\lambda - p_3 p_2 - 2p_3)\, w^2 + \left[\lambda^2(1 - p_3^2) + \lambda\, p_3(p_1 p_3^2 - p_2) + p_3^2(1 + 2p_2) - 3p_1 p_3 + p_2 - 1\right] w + \\ &+ \lambda(p_2 - p_1 p_3 - p_2 p_3^2 + p_1 p_3^3) - p_1 + p_2(1 - p_2)p_3 + p_1(1 + 2p_2)p_3^2 - (p_1^2 + p_2)p_3^3, \end{aligned} \tag{35}$$

whereas the characteristic polynomial $P_Z(z; \lambda)$ of Z reads

$$P_Z(z;\lambda) = z^3 + 2\lambda z^2 + (\lambda^2 + p_2 - 1)z + p_2\lambda - p_1. \tag{36}$$

The differences in (31),

$$k_j = w_{j+1} - w_{j+2}, \quad \omega_j = z_{j+1} - z_{j+2}, \quad j = 1, 2, 3 \quad \mathrm{mod}(3), \tag{37}$$

play the roles of "eigen-wave numbers" and "eigen-frequencies", respectively. We observe that the matrices W and Z are related to one another as follows:

$$W = p_3 Z^2 + (1 + p_3\lambda)Z + p_2 p_3. \tag{38}$$

This induces a relation between the eigenvalues w_j and z_j so that

$$k_j = \omega_j\left[-p_3 z_j + (1 - \lambda p_3)\right], \quad j = 1, 2, 3. \tag{39}$$

Given p_1, p_2 and p_3, we are interested in finding values of the complex spectral parameter λ such that the locally perturbed plane waves u_j are bounded in space, and see if they are linearly stable or unstable in time. In other words, we look for those values of λ corresponding to real eigen-wave numbers k_j; to such eigen-wave numbers there correspond in general complex eigen-frequencies ω_j: if the imaginary part of ω_j is nonzero, linear instability develops in time.
The stability spectrum $\mathbf{S}$ for the plane wave solutions of the 3WRI system (1) is defined as the locus of the λ-plane identified with $\mathbb{C}$ such that, for fixed values of the physical parameters p_1, p_2 and p_3, there exist at least two eigenvalues w_ℓ and w_m for the matrix W, for some ℓ and m, for which $(w_\ell - w_m) \in \mathbb{R}$ (namely, for which one of the k_j is real).

The key-concept in understanding the linear stability is the difference of the eigenvalues w_j, which is related to the difference of the eigenvalues z_j via (39). Indeed, it is possible to show [48] that

Proposition 1. *The plane wave solution of the 3WRI system is stable against the perturbation δU integrated over strictly real values of λ (see 18), with the exception of a finite number of intervals on the real line, called gaps, and possibly of isolated, real points within such gaps.*

Following [44], we construct the cubic polynomial $\mathcal{P}_W(\xi;\lambda) \equiv \mathcal{P}_W(\xi;\lambda;p_1,p_2,p_3)$ in the variable ξ, whose ξ-roots are the squares of all the possible differences of the roots of the characteristic polynomial $P_W(w;\lambda)$ (35), namely

$$\mathcal{P}_W(\xi;\lambda) \equiv \mathcal{P}_W(\xi;\lambda;p_1,p_2,p_3) = \prod_{\substack{j,h=1\\ j<h}}^{3} \left[\xi - (w_j - w_h)^2\right]. \tag{40}$$

A ξ-root (resp. a λ-root) of $\mathcal{P}_W(\xi;\lambda)$ is a polynomial root of the equation $\mathcal{P}_W(\xi;\lambda) = 0$, solved with respect to ξ (resp. λ). For the sake of simplicity, we will refer to $\mathcal{P}_W(\xi;\lambda)$ as the *polynomial of the squares of the differences*; it is a 2-variate polynomial in ξ and λ, which can be explicitly obtained in terms of the coefficients of $P_W(w;\lambda)$ (see [44,48]), and takes the expression:

$$\begin{aligned}\mathcal{P}_W(\xi;\lambda) = {}& \xi^3 + \xi^2\left[2\lambda p_3(3p_1p_3 + p_2 + 8) - 18p_1p_3 - 2(p_2-1)^2p_3^2 + 6(p_2-1) - 2\lambda^2\left(3p_3^2+1\right)\right] + \\ & + \xi\left\{-\lambda p_3(3p_1p_3 + p_2 + 8) + 9p_1p_3 + p_2\left[(p_2-2)p_3^2 - 3\right] + \lambda^2\left(3p_3^2+1\right) + p_3^2 + 3\right\}^2 + \\ & + \left\{-4\lambda^4 + 27p_1^2 + 4\lambda^3p_1 - 18\lambda p_1(p_2+2) + \lambda^2\left[8-(p_2-20)p_2\right] + 4(p_2-1)^3\right\} \times \\ & \times \left\{p_3\left[\lambda + p_3^2(p_1-\lambda) - p_2p_3 + p_3\right] - 1\right\}^2 .\end{aligned} \tag{41}$$

Therefore, for any fixed parameters p_1, p_2 and p_3, the spectrum $\mathbf{S}$ is the locus of the λ-roots of $\mathcal{P}_W(\xi;\lambda)$ for all $\xi \in \mathbb{R}$, $\xi \geq 0$, that is

$$\mathbf{S} = \{\lambda \in \mathbb{C} \,|\, \mathcal{P}_W(\xi;\lambda) = 0,\, \xi \geq 0\}. \tag{42}$$

The stability spectrum $\mathbf{S}$ of the solution U coincides with the subset of the complex λ-plane over which the integration (18) runs. This subset guarantees the boundedness of the solution F, and hence that of the perturbation δU. We are now in the position to redefine the perturbation in (18) as

$$\delta U(x,t) = \int_{\mathbf{S}} d\lambda\, F(x,t,\lambda). \tag{43}$$

As in standard linear stability analysis, the given solution U is linearly stable if the initial perturbation $\delta U(x,t_0)$ remains small as time grows, say for $t > t_0$.
In the following section, we classify the stability spectra $\mathbf{S}$ in the parameter space.

3. Classification of stability spectra S

As we will illustrate in this section, the topological features of the spectrum $\mathbf{S}$ can be classified as follows. Real values of the spectral parameter λ not belonging to $\mathbf{S}$ constitute a *gap* (G). A gap, containing an isolated point belonging to $\mathbf{S}$, is called a *split gap* (SG). Non-real values of the spectral parameter λ, belonging to $\mathbf{S}$, correspond to *branches* (B) and *loops* (L), which are open and closed curves, respectively. Figure-eight shaped loops, self-intersecting on the real axis, will be referred to as *twisted loops* (TL).
In order to classify the topological features of $\mathbf{S}$, we need to investigate the algebraic properties of the polynomial of the squares of the differences $\mathcal{P}_W(\xi;\lambda)$, defined in (40), which is a sixth degree polynomial in λ and a third degree polynomial in ξ. For fixed p_1, p_2 and p_3, we analyse the spectrum $\mathbf{S}$ following

the approach introduced in [44,46] for the CNLS equations, and further investigated in [48] for the case of the 3WRI system.
As explained in [44,46], the different components of the stability spectrum **S** result from the dynamics of the λ-roots of $\mathcal{P}_W(\xi;\lambda)$ as ξ varies from 0 to ∞; in particular, the components are generated by collisions on the real axis of pairs of λ-roots, whenever after such collisions the colliding roots either leave or go into the real axis. In other words, collisions corresponding to real roots passing each other on the real axis are disregarded, as they do not originate additional components of the curve **S**.
To analyse these collisions, we consider the discriminant of $\mathcal{P}_W(\xi;\lambda)$ with respect to λ, that is

$$\mathcal{Q}(\xi;p_1,p_2,p_3) = \Delta_\lambda\, \mathcal{P}_W(\xi;\lambda) = \xi\, \mathcal{Q}_1^2(\xi)\, \mathcal{Q}_2(\xi), \tag{44}$$

where $\mathcal{Q}_1(\xi) \equiv \mathcal{Q}_1(\xi;p_1,p_2,p_3)$ and $\mathcal{Q}_2(\xi) \equiv \mathcal{Q}_2(\xi;p_1,p_2,p_3)$ are two real polynomials in the variable ξ, whose degrees are four and six, respectively, and $\mathcal{Q}_{1,2}(0) \neq 0$. The explicit forms of $\mathcal{Q}_1(\xi)$ and $\mathcal{Q}_2(\xi)$ are too long for the present paper and can be found in [48]. We will refer to $\mathcal{Q}_1$ and $\mathcal{Q}_2$ as the *even* and *odd* parts of the discriminant $\mathcal{Q}(\xi)$, respectively. We are interested in changes of sign of $\mathcal{Q}(\xi;p_1,p_2,p_3)$.
If $\xi > 0$, the factor $\xi\mathcal{Q}_1^2(\xi)$ is strictly positive and so, to the purpose of the study of the sign of the discriminant $\mathcal{Q}(\xi)$, the only relevant part is $\mathcal{Q}_2(\xi)$. As ξ varies towards ∞, $\mathcal{Q}_2(\xi)$ will change sign each time ξ goes through a root of $\mathcal{Q}_2(\xi)$: therefore, to each choice of p_1, p_2 and p_3, there corresponds a sequence of intervals of ξ, where $\mathcal{Q}_2(\xi)$ is either positive or negative. In particular, the following proposition holds [44,48]:

Proposition 2. *Let $\bar{\xi}$ be the largest positive root of $\mathcal{Q}_2(\xi)$. Then, for $\xi > \bar{\xi}$, all the λ-roots of $\mathcal{P}_W(\xi;\lambda)$ are real; therefore, the stability spectra always contains part of the real axis and never features a gap containing the point at infinity.*

As p_1, p_2 and p_3 vary, transitions from a sequence of intervals in ξ to another correspond to one of the intervals shrinking to a point, namely to a collision of a pair of roots of $\mathcal{Q}_2(\xi)$. We therefore consider the discriminant of $\mathcal{Q}_2(\xi)$ with respect to ξ, $\Delta_\xi \mathcal{Q}_2(\xi)$, which factorises as

$$\Delta_\xi \mathcal{Q}_2(\xi) = \prod_{j=1}^{5} E_j(p_1,p_2,p_3)^{e_j}, \tag{45}$$

where E_j are polynomial factors and e_j are their multiplicities. Then, the real-analytic varieties $\mathcal{E}_j$ implicitly defined as

$$\mathcal{E}_j = \left\{(p_1,p_2,p_3) \in \mathbb{R}^3 \;:\; E_j(p_1,p_2,p_3) = 0\right\}, \quad j = 1,2,3,4,5, \tag{46}$$

are curves in the parameter space, defining the boundaries of regions corresponding to different topological structures of the spectra **S**. These are

$$E_1 = p_1 - p_2, \tag{47a}$$
$$E_2 = p_1 + p_2, \tag{47b}$$
$$E_3 = 27p_1^2 - (p_2-1)(p_2+8)^2, \tag{47c}$$
$$E_4 = p_3\left[p_3^3\left(p_1^2 - 4p_2 + 4\right) - 2p_1(p_2-2)p_3^2 - 4p_1 + (p_2(p_2+4)-8)p_3\right] + 4, \tag{47d}$$

and the explicitly expression of E_5 can be obtained from (45) knowing E_j, $j = 1,...,4$ (see [48]). All the multiplicities e_j are equal to 1, with the only exception of $e_3 = 3$.
For $\xi = 0$, $\mathcal{Q}(0) = 0$ and therefore it requires a different approach; we will study this case in the next subsection.

3.1. Gaps, branches and loops

As shown in [44,46], end points of gaps on the real line and of branches in the complex λ-plane correspond to setting $\xi = 0$ in $\mathcal{P}_W(\xi;\lambda)$, or equivalently, to multiple w-roots of the characteristic polynomial $P_W(w;\lambda)$.
When $\xi = 0$, it turns out that

$$\mathcal{P}_W(0;\lambda) = \mathcal{P}_Z(0;\lambda)\mathcal{R}^2(\lambda), \tag{48}$$

where $\mathcal{P}_Z(\zeta;\lambda)$ is the polynomial of the squares of the differences of the z-roots of $P_Z(z;\lambda)$,

$$\mathcal{P}_Z(0;\lambda) = -4\lambda^4 + 4p_1\lambda^3 - [(p_2-20)p_2 - 8]\,\lambda^2 - 18p_1(p_2+2)\lambda + 27p_1^2 + 4(p_2-1)^3, \tag{49}$$

and where

$$\mathcal{R}(\lambda) = p_3\left[(1-p_3^2)\lambda + p_1p_3^2 - p_2p_3 + p_3\right] - 1. \tag{50}$$

Gaps and branches appear or disappear at the multiple-zeros of the polynomial $\mathcal{P}_Z(0;\lambda)$, thus at the zeros of the discriminant $\Delta_\lambda\mathcal{P}_Z(0;\lambda)$, namely when

$$\Delta_\lambda\mathcal{P}_Z(0;\lambda) = -256(p_1-p_2)(p_1+p_2)\left[27p_1^2 - (p_2-1)(p_2+8)^2\right]^3 = -256\,E_1E_2E_3^3. \tag{51}$$

Indeed, as we will see later in this section, $\mathcal{R}(\lambda)$ does not play a role in the classification of gaps and branches, but it provides conditions for the existence of split-gaps. The curves $\mathcal{E}_j$ associated with the three polynomial factors E_j in (51), with $j = 1,2,3$, bound the regions in the (p_1,p_2)-plane characterised by different numbers of gaps and branches. Following this observation, we will classify the spectra fixing the parameter p_3 and varying p_1, p_2 (this is trivial as long as one is interested only in $\mathcal{E}_1$, $\mathcal{E}_2$ and $\mathcal{E}_3$, which do not depend on p_3, but it informs our approach in view of the full classification, when $\mathcal{E}_4$ and $\mathcal{E}_5$ too are taken into account). In particular, we observe that the curves $\mathcal{E}_1$, $\mathcal{E}_2$ and $\mathcal{E}_3$ are the same that appear in the classification of gaps and branches of the CNLS system [44,46]. Consequently, as in [44,46], the following proposition holds:

Proposition 3. *The 3WRI plane wave solutions stability spectrum* **S** *has the gaps and branches structure described in Table below, where the symbol # stands for 'number of' and where E_3 is as in (47c).*

Regions on the (p_1,p_2)-plane	$\#G$	$\#B$	λ-roots of $\mathcal{P}_Z(0;\lambda)$
$0 < p_2 < E_3$ and $-p_2 < p_1 < p_2$	2	0	4 distinct and real
$E_3 < p_2 < p_1$ and $E_3 < p_1$	2	0	4 distinct and real
$E_3 < p_2 < -p_1$ and $E_3 < -p_1$	2	0	4 distinct and real
$p_2 > E_3$ and $-p_2 < p_1 < p_2$	1	1	2 distinct and real, 2 complex conjugate
$p_1 < p_2 < -p_1$ and $p_1 < 0$	1	1	2 distinct and real, 2 complex conjugate
$-p_1 < p_2 < p_1$ and $p_1 > 0$	1	1	2 distinct and real, 2 complex conjugate
$p_2 < 0$ and $p_2 < p_1 < -p_2$	0	2	2 pairs of complex conjugate

The structure of the gaps depends only on p_1 and p_2, see (47a), (47b) and (47c). Nevertheless, because of the relation (48), $\mathcal{P}_W(0;\lambda)$ can be zero also when $\mathcal{R}(\lambda) = 0$, namely when

$$\lambda = \frac{p_3^2(p_1p_3 - p_2 + 1) - 1}{p_3\,(p_3^2 - 1)}. \tag{52}$$

This corresponds to a double-root of $\mathcal{P}_W(0;\lambda)$. Since, $\mathcal{R}(\lambda)$ is a first degree polynomial and it has real coefficients, the equality $\mathcal{R}(\lambda) = 0$ may be verified just in one point of the real spectrum **S**. Moreover, for values of p_1 and p_2 varying in an interval without changing the number of gaps, this point can move inside a gap or can coincide with the endpoint of a gap, depending on p_3. In other words, we expect that the regions in the (p_1,p_2)-plane in which the zero of $\mathcal{R}(\lambda)$ is inside a gap move by varying p_3. A tedious

but easy calculation reveals that when $\mathcal{R}(\lambda) = 0$, $\mathcal{P}_Z(0;\lambda)$ can be either positive or zero (see 49), (50); we have only two possible scenarios:

1. $\mathcal{R}(\lambda) = 0$ with $\mathcal{P}_Z(0;\lambda) > 0$: the double-zero (52) falls within a gap, namely, the spectrum features a split-gap;
2. $\mathcal{R}(\lambda) = 0$ with $\mathcal{P}_Z(0;\lambda) = 0$: the double-zero(52) is a triple-zero of the polynomial $\mathcal{P}_W(0;\lambda)$ and it coincides with the endpoint of a gap.

Thus, the condition for existence of a split-gap can be obtained by studying when the resultant with respect to λ of $\mathcal{P}_Z(0;\lambda)$ and $\mathcal{R}(\lambda)$ is zero, namely $\mathrm{Res}_\lambda(\mathcal{P}_Z(0;\lambda), \mathcal{R}(\lambda)) = 0$. The expression of this resultant contains two polynomial factors: a squared polynomial, which does not change sign and does not correspond to any transition, while the other coincides with $-E_4$ (see (47d)). Consequently, we have

Proposition 4. *Fixing the parameter p_3, the curve $\mathcal{E}_4$ (47d), identifies in the (p_1, p_2)-plane the transition curve for the existence of split gap. In particular, fixing the values of p_3, the values of the parameters p_1 and p_2 for which the polynomial E_4 is negative correspond to regions where there is a split gap.*

Proof. Recall the expressions of $\mathcal{P}_Z(0;\lambda)$ and $\mathcal{R}(\lambda)$ in (49) and (50), respectively, and let τ_j and θ be their roots, so that the resultant with respect to λ can be written as

$$\mathrm{Res}_\lambda(\mathcal{P}_Z(0;\lambda), \mathcal{R}(\lambda)) = -4\, p_3^4 (1 - p_3^2)^4 \prod_{k=1}^{4} (\tau_k - \theta). \tag{53}$$

Let us suppose, say, τ_j are all real and distinct, such that we have two gaps; without loss of generality we assume $\tau_1 < \tau_2 < \tau_3 < \tau_4$. If θ coincides with the end point of a gap, so that $\theta = \tau_j$ for some j, then the resultant (53) vanishes. If, instead, θ falls within a gap, that is $\tau_1 < \theta < \tau_2 < \tau_3 < \tau_4$ or $\tau_1 < \tau_2 < \tau_3 < \theta < \tau_4$, namely if we have a split-gap, then the resultant (53) is positive. Since the resultant can be factorised as a squared polynomial times $-E_4$, this implies $E_4 < 0$. Finally, if θ falls between two gaps, that is $\tau_1 < \tau_2 < \theta < \tau_3 < \tau_4$, then the resultant in (53) is negative, and $E_4 > 0$. The same argument can be straightforwardly extended to the case of two distinct real roots and of two complex conjugate roots. □

By taking into account the regions associated with split-gaps, one has the following Proposition.

Proposition 5. *Fixing the parameter p_3, split-gaps exist in the regions defined as follows:*

1. *If $-1 < p_3 < 1$, $\sigma_1 < p_1 < \sigma_2$ and $p_2 > 1 - \frac{1}{p_3^2}$;*
2. *If $p_3 < -1$ or $p_3 > 1$, $\sigma_1 < p_1 < \sigma_2$ and $p_2 > 1 - \frac{1}{p_3^2} > 0$;*

where $\sigma_1 = \frac{2}{p_3^3} + \frac{p_2 - 2}{p_3} - \frac{2|p_3^2 - 1|\sqrt{1 + (p_2 - 1)p_3^2}}{|p_3|^3}$, $\sigma_2 = \frac{2}{p_3^3} + \frac{p_2 - 2}{p_3} + \frac{2|p_3^2 - 1|\sqrt{1 + (p_2 - 1)p_3^2}}{|p_3|^3}$.

To classify gaps as p_3 changes, we take advantage of the symmetries in the (p_1, p_2)-plane. Indeed, since $\Delta_\lambda \mathcal{P}_Z(0;\lambda)$ in (51) is invariant under transformations $p_1 \to -p_1$ and $p_2 \to p_2$, the curves $\mathcal{E}_1$, $\mathcal{E}_2$ and $\mathcal{E}_3$ are symmetric with respect to the p_2-axis. The curve $\mathcal{E}_4$ depends also on p_3, and it has symmetries $p_1 \to -p_1$, $p_2 \to p_2$ and $p_3 \to -p_3$. In particular, by changing p_3 into $-p_3$, the curve $\mathcal{E}_4$ is reflected with respect to the p_2-axis. Therefore, following Proposition 5, in order to understand the regions in the (p_1, p_2)-plane associated with different numbers of gaps, branches and split gaps, it is sufficient to consider the two cases, $|p_3| > 1$ and $0 < |p_3| < 1$ (see Fig. 1).

So far we have considered the case $\xi = 0$ in which at least two w-roots of the characteristic polynomial $P(w;\lambda)$ coincide. Considering the λ-roots of the polynomial $\mathcal{P}_Z(0;\lambda)$, this case can be summarised as follows: 4 distinct real roots, or 2 distinct real roots and 1 double real root (2G 0B or 1G 1SG 0B); 2 distinct real roots and 2 complex conjugate roots, or 1 double root and 2 complex conjugate roots (1G 1B or 0G 1SG 1B); 2 pairs of complex conjugate roots (0G 2B), see Proposition 3.

Let us consider the polynomial $\mathcal{P}_W(\xi;\lambda)$ for $\xi > 0$. As we have observed at the beginning of Sect. 3, this case can be studied by analysing $\mathcal{Q}_2(\xi)$, requiring also the inclusion of the curve $\mathcal{E}_5$ in the (p_1, p_2), for

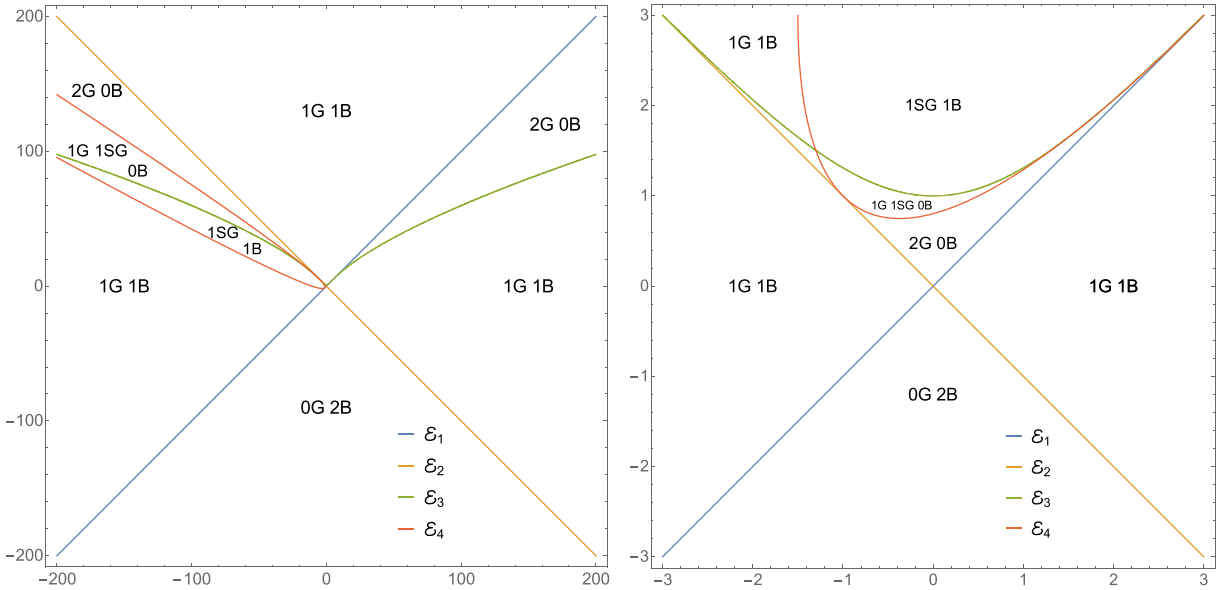

FIG. 1. Regions in the (p_1, p_2)-plane (p_1 on the horizontal axis, p_2 on the vertical axis) associated with different numbers of gaps (G), branches (B) and split gaps (SG), for $p_3 = -0.6$ (left) and $p_3 = 2$ (right). The gap-branch topology of the small, unlabelled region bounded by $\mathcal{E}_2$, $\mathcal{E}_3$ and $\mathcal{E}_4$, in the plot on the right, is 2G 0B

a fixed p_3, when defining the bounding regions of different topology. In particular, the only additional features of the spectrum $\mathcal{S}$ that form for $\xi > 0$ are closed continues curves that start and end on the real axis. They come in two different kinds: loops and twisted loops. Loops are generated by a pair of real λ-roots, which collide for some value of $\xi > 0$ and scatter into the complex plane as a pair of complex conjugate roots, as ξ increases, to collide again on the real axis for another, larger, value of ξ. Twisted loops are figure-eight shaped loops, self-intersecting on the real axis. The self intersection point of the twisted loop corresponds to the double λ-root (52) and thus corresponds to the isolated point within a split-gap (subfigure on the left of Fig. 4, Fig. 5 and subfigure on the left of Fig. 6).
Adopting the same approach as in [46], the following relations linking the number of branches, loops and twisted loops can be derived:

$$\#TL + 2\#L + \#B = \#\xi^+, \quad \#G + 2\#SG = \#\xi^-, \quad 4 - 2\#L - 2\#TL = \#\xi_{cc}, \tag{54}$$

where ξ^+, ξ^- and ξ_{cc} stand for the positive, negative and complex conjugate ξ-roots of the polynomial $\mathcal{Q}_2(\xi)$, and where the symbol # stands for 'number of'. Moreover, since $\mathcal{Q}_2(\xi)$ is a sixth degree polynomial, the relation $\#\xi^+ + \#\xi^- + \#\xi_{cc} = 6$ must be verified. This implies that, because of (54) and keeping in mind that $\#TL = \#SG$, we have also

$$\#SG + \#G + \#B = 2. \tag{55}$$

Proposition 6. *The different typologies of stability spectra of the* 3 *WRI system (1) are given in the Table below.*

Finally, besides the symmetries of the curves on the (p_1, p_2)-plane, we observe that the polynomial $\mathcal{Q}_2(\xi)$ is invariant under the simultaneous transformations $p_1 \to -p_1$ and $p_3 \to -p_3$. This invariance, together with the symmetry of the curve $\mathcal{E}_4$, which is reflected with respect to the p_2-axis when p_3 goes $-p_3$, entails that the regions of different topologies listed in Proposition 6 are simply reflected about the p_2-axis on

Topological structures	$\#\xi^+$, $\#\xi^-$, $\#\xi_{cc}$
1G 1B 2L	5, 1, 0
1G 1B 1L	3, 1, 2
1G 1B 0L	1, 1, 4
0G 2B 2L	6, 0, 0
0G 2B 1L	4, 0, 2
0G 2B 0L	2, 0, 4
2G 0B 2L	4, 2, 0
2G 0B 1L	2, 2, 2
1G 1SG 0B 1L 1TL	3, 3, 0
0G 1SG 1B 1L 1TL	4, 2, 0
0G 1SG 1B 0L 1TL	2, 2, 2

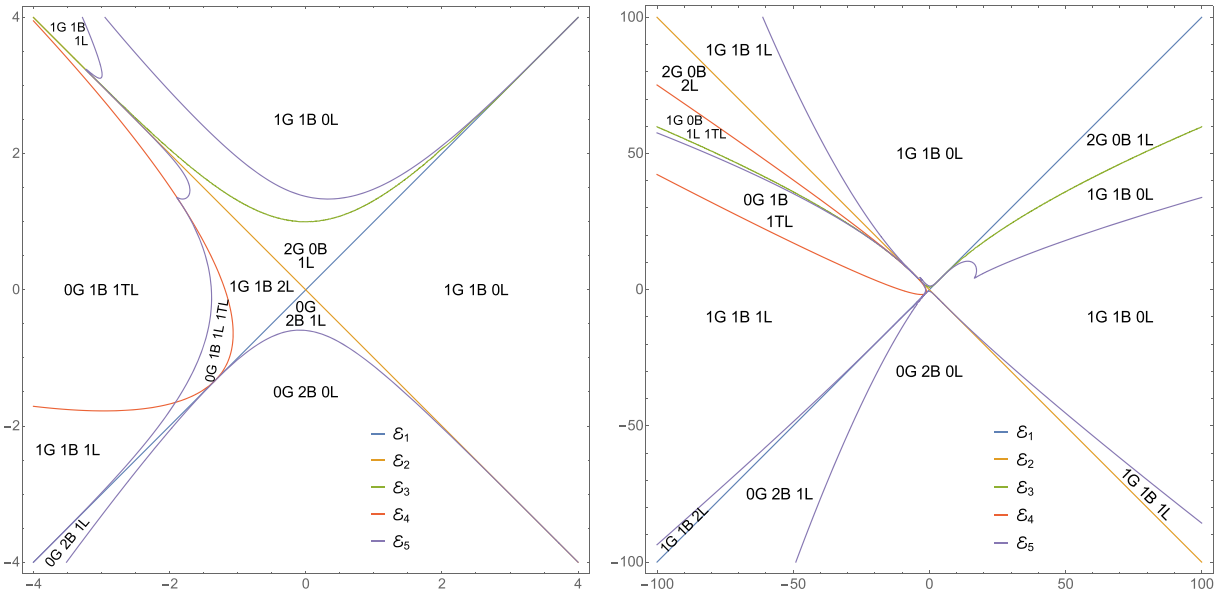

FIG. 2. The figure on the left displays regions of different topology in the (p_1, p_2)-plane (p_1 on the horizontal axis, p_2 on the vertical axis) for $p_3 = -0.6$, when $-4 < p_1 < 4$ and $-4 < p_2 < 4$. The topology of the unlabelled region bounded by $\mathcal{E}_3$ and the convex component of $\mathcal{E}_5$ bounding the 1G 1B 0L region is also 1G 1B 0L. If a region without a label is reached by crossing a component of the curve $\mathcal{E}_4$ starting from a neighbouring region with a label, then the topology of the region without label coincides with the topology of the region with a label that one started from, but with the number of gaps increased by one and one twisted-loops replaced by a loop. The figure on the right displays regions of different topology in the (p_1, p_2)-plane (p_1 on the horizontal axis, p_2 on the vertical axis) for $p_3 = -0.6$, when $-100 < p_1 < 100$ and $-100 < p_2 < 100$. The topology of the very narrow region on the left, bounded by $\mathcal{E}_3$ and $\mathcal{E}_5$, is 0G 1B 1TL. In both figures, the labels do not include the counting of the split gaps, as this always coincides with the number of twisted loops

the (p_1, p_2)-plane if we exchange p_3 with $-p_3$. For this reason, in view of the classification of the loops, in Figs. 2 and 3 below, we choose one value of p_3, namely $p_3 = -0.6$.

3.2. Gain function

The solution U is linearly stable if the initial perturbation $\delta U(x, t_0)$ remains small as time grows, say for $t > t_0$. The expression of the perturbation δU is given via the matrix F in (43), where F is a linear

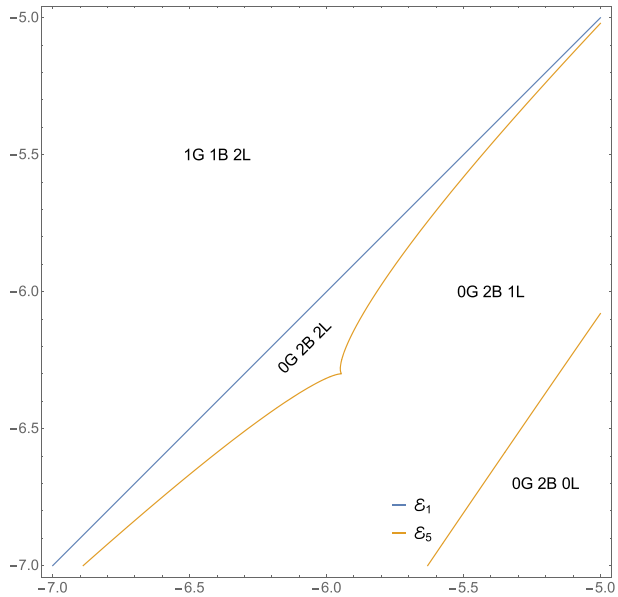

FIG. 3. Regions of different topology in the (p_1, p_2)-plane (p_1 on the horizontal axis, p_2 on the vertical axis) for $p_3 = -0.6$, when $-7 < p_1 < -5$ and $-7 < p_2 < -5$. This plot is a magnification of the 0 G 2B 2 L region displayed in the previous figure, which would otherwise be too small to be properly visualised and labelled

combination of the "Fourier-like modes $e^{i(xk_j - t\omega_j)}$. Let w_1 and w_2 denote the two eigenvalues of W such that their difference $k_3 = w_1 - w_2$ is real. For $\lambda \in \mathbf{S}$, let k_3 be the real eigen-wave-number and ω_3 is the corresponding eigen-frequency. Since $\omega_3(k_3)$ is in general complex, its imaginary part represents the growth rate of the perturbation, which we will denote as $\Gamma(k_3)$. Then, if $\omega_3(k_3)$ is strictly real, that is $\Gamma(k_3) = 0$ for all k_3 real, the system is linearly stable. On the contrary, if $\omega_3(k_3)$ is non-real, that is $\Gamma(k_3) \neq 0$ for some k_3, then the solution F, and so the perturbation δU, grows in time, leading to the linear instability of the system. We define the gain function $|\Gamma(k_3)|$ as the absolute value of the growth rate, and we say that when the gain function is positive for some values of k, then the system is linearly unstable for those wave numbers.

The gain function can be computed by constructing an implicit relation, linking the eigen-frequencies ω to the eigen-wave-number k. This can be obtained as follows: we start by constructing the ideal generated by

$$\left\{\mathcal{P}_W(k^2;\lambda),\, \mathcal{P}_Z(\omega^2;\lambda),\, \mathcal{C}(\omega;\sigma),\, \mathcal{S}_Z(\sigma;\lambda)\right\}$$

where $\mathcal{P}_W(k^2;\lambda) \equiv \mathcal{P}_W(\xi;\lambda)$, $\mathcal{P}_Z(\omega^2;\lambda) \equiv \mathcal{P}_Z(\zeta;\lambda)$ are the polynomials of the square of the differences of the eigenvalues of W and Z, respectively, $\mathcal{C}_Z(\omega;\sigma) = p_3\,\omega\,\sigma + (1+p_3)\,\omega + p_2\,p_3 - k$ is the Cayley-Hamilton relation obtained from (38), and $\mathcal{S}_Z(\sigma;\lambda) = \sigma^3 + 4\lambda\sigma^2 + \left(5\lambda^2 + p_2 - 1\right)\sigma + p_1 + \lambda\left(-2 + p_2 + 2\lambda^2\right)$ is the polynomial whose roots are the sums of the pairs of eigenvalues z_j of Z, so that the three σ-roots are $\sigma_1 = z_2 + z_3$, $\sigma_2 = z_3 + z_1$ and $\sigma_3 = z_1 + z_2$.

We then apply the Buchberger's algorithm to compute the Gröbner basis for the ideal (see, e.g., [49]), so to obtain a polynomial in the new basis featuring only k and ω^2. This polynomial reads as follows:

$$\begin{aligned}
&\mathcal{H}(\omega,k) = \\
&= k^4\left(\omega^2-4\right) - 4k^3\omega\left(p_1p_3+\omega^2-4\right) - k^2\omega^2\left[p_3^2\left(p_2^2+4p_2+2\omega^2-8\right) - 12p_1p_3 - 6\left(\omega^2-4\right)\right] + \\
&+ 2k\omega^3\left\{p_1p_3\left[(2-p_2)p_3^2-6\right] + p_3^2\left(p_2^2+4p_2+2\omega^2-8\right) - 2\omega^2 + 8\right\} + \\
&+ \omega^4\left\{p_3^4\left(4p_2-p_1^2-4\right) + 2p_1(p_2-2)p_3^3 + 4p_1p_3 - \left[p_2(p_2+4)-8\right]p_3^2 - 4\right\} + \left(p_3^2-1\right)^2\omega^6. \qquad (56)
\end{aligned}$$

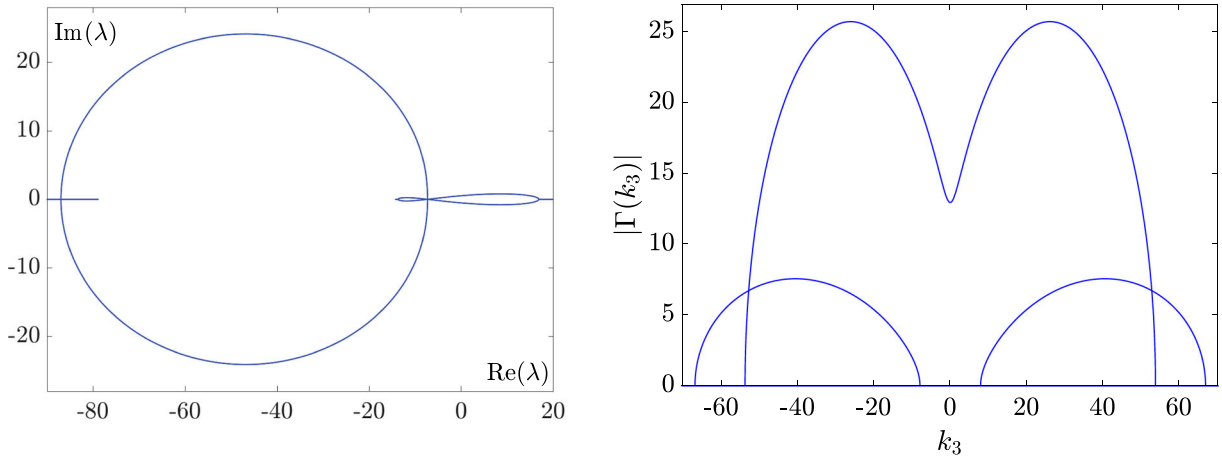

FIG. 4. Stability spectrum (left) with 1 G 1SG 0B 1 L 1TL, obtained for $p_1 = -90$, $p_2 = 60$, $p_3 = -0.6$ and its associated gain function (right). As it is always observed numerically in the case of stability spectra with twisted-loops and split-gaps, the gain function features a nonzero component in the neighbourhood of the zero wave-number. The passband-type instability is associated with the presence of a loop in the stability spectrum

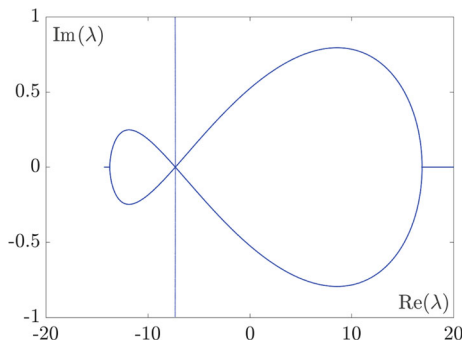

FIG. 5. Zoom-in of the twisted-loop and split-gap in the stability spectrum with 1 G 1SG 0B 1 L 1TL, obtained for $p_1 = -90$, $p_2 = 60$, $p_3 = -0.6$, as displayed in Fig. 4

For a fixed eigen-wave-number k_3, the three ω-roots of

$$\mathcal{H}(\omega, k_3) = 0$$

are the three possible values of the eigen-frequency ω_3. The multi-valuedness of $\omega_3(k_3)$ results from the polynomial of the square of the differences $\mathcal{P}_W(\xi;\lambda)$ being of degree six, and thus entailing six values of λ for a given k_3. By writing the equations for the real and imaginary part of ω in $\mathcal{H}(\omega, k) = 0$, and of λ in $\mathcal{P}(k^2, \lambda)$, one obtains a system of four real equations for four real unknowns. By analysing this latter system, it is then possible to show that, if p_1, p_2 and p_3 are such that $E_j \neq 0$, $j = 1, 2, 3$, then the imaginary part of ω_j is zero, for $j = 1, 2, 3$ and for all $k > 0$, only if the imaginary part of λ is zero for all k (see [48] for details). This leads to the following Proposition:

Proposition 7. *For a generic choice of p_1, p_2 and p_3 (i.e. such that $E_j \neq 0$), the plane wave solution of the 3 WRI system (1) is linearly unstable.*

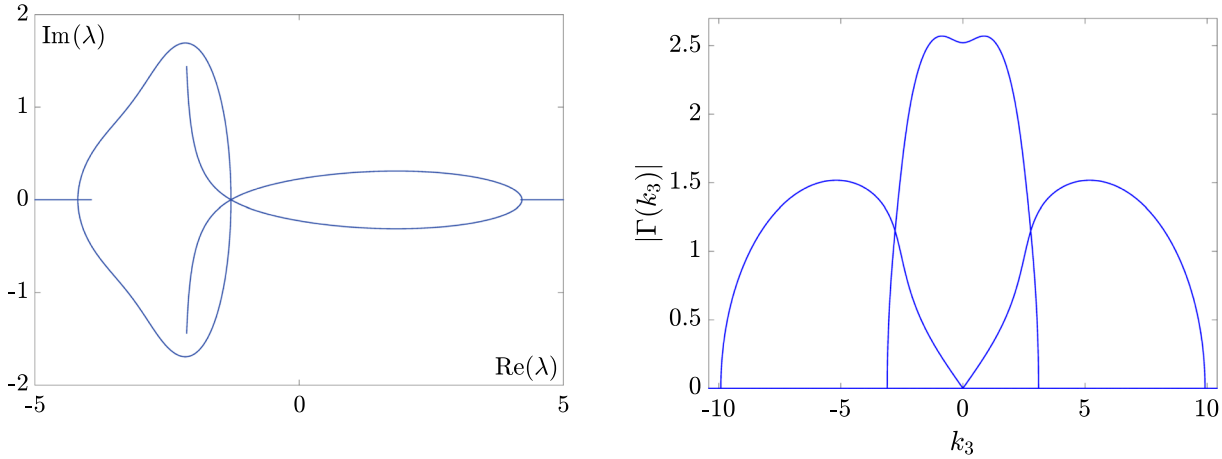

FIG. 6. Stability spectrum (left) with 0 G 1SG 1B 0 L 1TL obtained for $p_1 = -4$, $p_2 = 2$, $p_3 = -0.6$ and its associated gain function (right). As it is always observed numerically in the case of stability spectra with twisted-loops and split-gaps, the gain function features a nonzero component in the neighbourhood of the zero wave-number. The baseband-type instability is associated with the presence of a branch in the stability spectrum

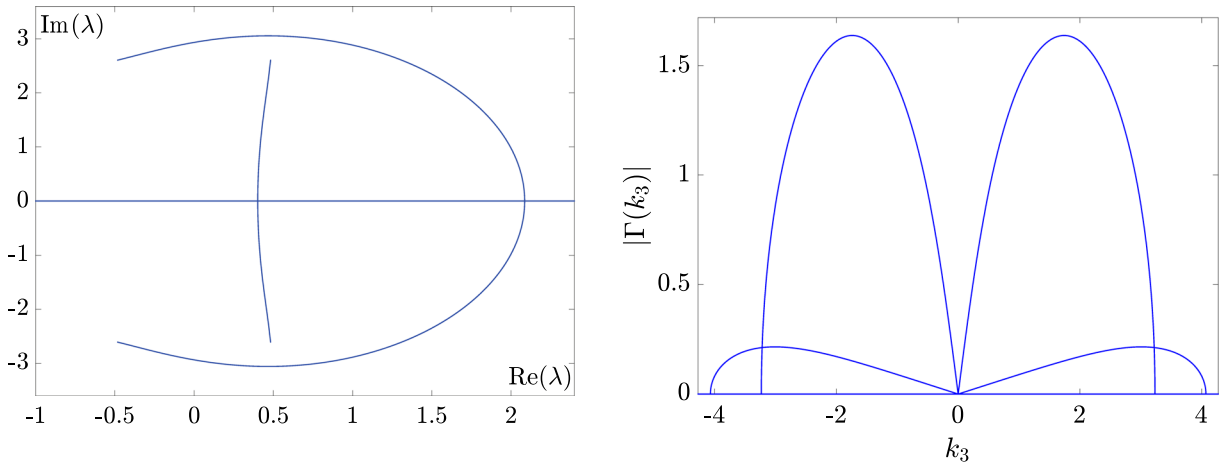

FIG. 7. Stability spectrum (left) with 2B 0 G 0 L obtained for $p_1 = 0$, $p_2 = -8/3$, $p_3 = 3/5$ and its associated gain function (right). The baseband-type instability featured by the gain function corresponds to the existence of two branches in the spectrum

4. Conclusions

We provide a classification of the stability spectra for the 3WRI system in the parameters space, and for each spectrum, we give the associated gain function. We find that for a generic choice of the parameters p_1, p_2 and p_3, the plane wave solution of the 3WRI system is linearly unstable (see Proposition 7). The parameters p_j are related to the physical parameters (amplitudes a_j, velocities c_j and signs s_j, $j = 1, 2, 3$) via the formulae (34) (Figs. 4, 5, 6).

In analogy to the CNLS system where baseband MI is believed to be a sufficient and necessary condition for the onset of rogue wave-type localised peaks [27,28,50], we speculate that linear instability of baseband type can be a necessary condition for the same phenomenology in the 3WRI system, that

is, the linear stability analysis of the system provides information about its subsequent nonlinear evolution. For instance, the plane wave solution used as a seed in the Darboux transformation generating the bright-dark-bright rogue wave triplet in the middle column of Figure 15 in [51], corresponds to a stability spectrum of 2B 0G 0L type (see Fig. 7), $p_1 = 0.0$, $p_2 = -8/3$ and $p_3 = 3/5$, i.e., $c_1 = 4$, $c_2 = 1$, $a_1 = 1/2\sqrt{3}$, $a_2 = 2/\sqrt{3}$ and $s_1 = s_3 = -s_2$. Along this line, we have carried out preliminary numerical tests by numerically integrating, via the method of lines, the initial value problem from perturbed plane waves with different kinds of perturbations at time $t = 0$. We observe that, when the plane waves solution is associated with a spectrum that does not feature branches or twisted loops, namely when the gain function has only passband components, a random perturbation develops as a wave train. On the contrary, if the corresponding spectrum features at least one branch and no twisted loops, namely if the gain function has a baseband component, then a random perturbation develops as a series of space-time localised coherent structures. Finally, if the corresponding spectrum features a twisted loop, we observe that the gain function has neither a baseband nor a passband component, being nonzero in the neighbourhood of the zero wave number. In this case, we consistently observe blow up at finite time in our numerical explorations. All this phenomenology, in particular the connection between twisted loops in the spectrum, blow-ups and explosive instability will be matter of future investigations.

Acknowledgements

SL, MR and MS are grateful, with the usual absolution from responsibility, to Antonio Degasperis, Gennady El and Karima Khusnutdinova for insightful discussions, and to Marcos Caso-Huerta for his comments and for proof-reading the manuscript. MR gratefully acknowledges financial support from Northumbria University in the form of a PhD scholarship. The work of MS and MR has been carried out under the auspices of the Italian GNFM (Gruppo Nazionale Fisica Matematica), INdAM (Istituto Nazionale di Alta Matematica), that is gratefully acknowledged.

Open Access. This article is licensed under a Creative Commons Attribution 4.0 International License, which permits use, sharing, adaptation, distribution and reproduction in any medium or format, as long as you give appropriate credit to the original author(s) and the source, provide a link to the Creative Commons licence, and indicate if changes were made. The images or other third party material in this article are included in the article's Creative Commons licence, unless indicated otherwise in a credit line to the material. If material is not included in the article's Creative Commons licence and your intended use is not permitted by statutory regulation or exceeds the permitted use, you will need to obtain permission directly from the copyright holder. To view a copy of this licence, visit http://creativecommons.org/licenses/by/4.0/.

Publisher's Note Springer Nature remains neutral with regard to jurisdictional claims in published maps and institutional affiliations.

References

[1] Zakharov, V.E., Manakov, S.V.: Resonant interaction of wave packets in nonlinear media. Pis'ma Zh. Eksp. Teor. Fiz. **18**, 413 (1973)
[2] Kaup, D.J.: The three-wave interaction-A nondispersive phenomenon. Stud. Appl. Math. **55**, 9–44 (1976)
[3] Kaup, D.J., Reiman, A., Bers, A.: Space-time evolution of nonlinear three-wave interactions. I. Interaction in a homogeneous medium. Rev. Mod. Phys. **51**(2), 275–310 (1979)
[4] Calogero, F., Degasperis, A.: Novel solution of the system describing the resonant interaction of three waves. Physica D **200**, 242–256 (2005)
[5] Conforti, M., Baronio, F., Degasperis, A., Wabnitz, S.: Inelastic scattering and interactions of three-wave parametric solitons. Phys. Rev. E **74**, 065602(R) (2006)
[6] Degasperis, A., Conforti, M., Baronio, F., Wabnitz, S., Lombardo, S.: The three-wave resonant interaction equations: spectral and numerical methods. Lett. Math. Phys. **96**(1–3), 367–403 (2011)
[7] Trillo, S.: Bright and dark simultons in second-harmonic generation. Opt. Lett. **21**(15), 1111–1113 (1996)

[8] Degasperis, A., Conforti, M., Baronio, F., Wabnitz, S.: Stable control of pulse speed in parametric three-wave solitons. Phys. Rev. Lett. **97**, 093901 (2006)
[9] Scott, A.C., Chu, F.Y.F., McLaughlin, D.W.: The soliton: a new concept in applied science. Proc. IEEE **61**(10), 1443 (1973)
[10] McCall, S., Hahn, E.: Self-induced transparency by pulsed coherent light. Phys. Rev. Lett. **18**, 908 (1967)
[11] Drühl, K., Wenzel, R.G., Carlsten, J.L.: Observation of solitons in stimulated Raman scattering. Phys. Rev. Lett. **51**, 1171 (1983)
[12] Picholle, E., Montes, C., Leycuras, C., Legrand, O., Botineau, J.: Observation of dissipative superluminous solitons in a Brillouin fiber ring laser. Phys. Rev. Lett. **66**, 1454 (1991)
[13] Baronio, F., Conforti, M., De Angelis, C., Degasperis, A., Andreana, M., Couderc, V., Barthélémy, A.: Velocity-locked solitary waves in quadratic media. Phys. Rev. Lett. **104**, 113902 (2010)
[14] Degasperis, A., Lombardo, S.: Rational Solitons of wave resonant-interaction models. Phys. Rev. E **88**, 052914 (2013)
[15] Zhang, G., Yan, Z., Wen, X.-Y.: Three-wave resonant interactions: multi-dark-dark-dark solitons, breathers, rogue waves, and their interactions and dynamics. Physica D **366**, 27–42 (2018)
[16] Yang, B., Yang, J.: General rogue waves in the three-wave resonant interaction systems. IMA J. Appl. Math. **86**(2), 378–425 (2021)
[17] Baronio, F., Conforti, M., Degasperis, A., Lombardo, S.: Rogue waves emerging from the resonant interaction of three waves. Phys. Rev. Lett. **111**, 114101 (2013)
[18] Müller, P., Garrett, C., Osborne, A.: Rogue waves. Oceanography **18**(3), 47 (2005)
[19] Horikis, T.P.: Rogue waves: extreme waves of water and light. J. Appl. Computer. Math. **3** (1), (2004)
[20] Tørum, A., Gudmestad, O.T.: Water Wave Kinematics. Kluwer Academic Publishers (1990)
[21] Erkintalo, M., Genty, G., Dudley, J.M.: Rogue-wave-like characteristics in femtosecond super continuum generation. Opt. Lett. **34**(16), 2468 (2009)
[22] Stenflo, L., Shukla, P.K.: Nonlinear acoustic gravity waves. J. Plasma Phys. **75**(6), 841–847 (2009)
[23] Bludov, Y.V., Konotop, V.V., Akhmediev, N.: Matter rogue waves. Phys. Rev. A. **80**(3), 033610 (2009)
[24] Shats, M., Punzmann, H., Xia, H.: Capillary Rogue Waves. Phys. Rev. Lett. **104**(10), 104503 (2010)
[25] Efimov, V.B., Ganshin, A.N., Kolmakov, G.V., McClintock, P.V.E., Mezhov-Deglin, L.P.: Rogue waves in superfluid helium. Eur. Phys. J. Spec. Top. **185**, 181–193 (2010)
[26] Lechuga, A.: Rogue waves in a wave tank: experiments and modelling. Nat. Hazards Earth Syst. Sci. **13**(11), 2951–2955 (2013)
[27] Baronio, F., Conforti, M., Degasperis, A., Lombardo, S., Onorato, M., Wabnitz, S.: Vector rogue waves and baseband modulation instability in the defocusing regime. Phys. Rev. Lett. **113**, 034101 (2014)
[28] Baronio, F., Chen, S., Grelu, P., Wabnitz, S., Conforti, M.: Baseband modulation instability as the origin of rogue waves. Phys. Rev. A **91**, 033804 (2015)
[29] Dudley, J.M., Dias, F., Erkintalo, M., Genty, G.: Instabilities, breathers and rogue waves in optics. Nature Photonics **8**, 755–764 (2014)
[30] Degasperis, A., Lombardo, S.: Multicomponent integrable wave equations: I. Darboux-dressing transformation. J. Phys. A: Math. Theor. **40**, 961–977 (2007)
[31] Degasperis, A., Lombardo, S.: Multicomponent integrable wave equations: II. Darboux-dressing transformation. J. Phys. A: Math. Theor. **42**(38), (2009)
[32] Gravilenko, V.G., Zelekson, L.A.: Resonant interaction of electromagnetic waves with an inhomogeneous stream of magnetized plasma. Radiophys. Quant. Electron. **20**, 679–682 (1977)
[33] Coppi, B., Rosenbluth, M.N., Sudan, R.N.: Nonlinear interactions of positive and negative energy modes in Rarefield plasmas. Ann. Phys. **55**, 207–247 (1969)
[34] Armstrong, J.A., Bloembergen, N., Ducuing, J., Persian, P.S.: Interactions between light waves in a nonlinear dielectric. Phys. Rev. **127**, 1918,15 (1962)
[35] Longuet-Higgins, M.S., Gill, A.E.: Resonant interactions between planetary waves. Proc. R. Soc. A **299**(1456), 120 (1967)
[36] Craik, A.D.D.: Wave interactions and fluid flows. Cambridge University Press (1985)
[37] Pan, Q., Peng, N.N., Chan, H.N., Chow, K.W.: Coupled triads in the dynamics of internal waves: case study using a linearly stratified fluid. Phys. Rev. Fluids **6**, 024802 (2021)
[38] Zakharov, V.E., Ostrovsky, L.A.: Modulation instability: the beginning. Physica D **238**, 540–548 (2009)
[39] Griffiths, S.D., Grimshaw, R.H.J., Khusnutdinova, K.R.: Modulational instability of two pair of counter-propagating waves and energy in a two-component system. Physica D Nonlinear Phenomena **214**(1), 1–24 (2005)
[40] Griffiths, S.D., Grimshaw, R.H.J., Khusnutdinova, K.R.: The influence of modulation instability on energy exchange in coupled sine-Gordon equations. Theor. Math. Phys. **137**(1), 1448–1458 (2003)
[41] Khusnutdinova, K.R.: Coupled Klein-Gordon equations and energy exchange in two-component system. Eur. Phys. J. Spec. Top. **147**, 45–72 (2007)
[42] Buckingham, R.J., Jenkins, R.M., Miller, P.D.: Semiclassical solitons ensembles for the three-wave resonant interaction equations. Commun. Math. Phys. **354**(3), 1015–1100 (2017)

[43] Degasperis, A., Lombardo, S.: Integrability in action: solitons, instability and rogue waves. Rogue Shock Waves Nonlinear Dispers. Media Part Lecture Notes Phys. Book Series **926**, 23–53 (2016)
[44] Degasperis, A., Lombardo, S., Sommacal, M.: Integrability and linear stability of nonlinear waves. J. Nonlinear Sci. **28**(4), 1251–1291 (2018)
[45] Caso-Huerta, M., Degasperis, A., Lombardo, S., Sommacal, M.: A new integrable model of long wave-short wave interaction and linear stability spectra. Proc. R. Soc. A **477**, 20210408 (2021)
[46] Degasperis, A., Lombardo, S., Sommacal, M.: Coupled nonlinear Schrödinger equations: spectra and instabilities of plane waves, Chapter B1, Nonlinear Systems and Their Remarkable Mathematical Structures: Volume 2, edited by N. Euler, M. C. Nucci (2019)
[47] Ablowitz, M.J., Kaup, D.J., Newell, A.C., Segur, H.: The inverse scattering transform—Fourier analysis for nonlinear problems. Stud. Apple. Math. **53**, 249–315 (1974)
[48] Romano, M.: The 3-Wave Resonant Interaction Model: Spectra and Instabilities of Plane Waves, PhD Thesis, Northumbria University (2019)
[49] Cox, D.A., Little, J., O'Shea, D.: Ideals, varieties, and algorithms, Springer (2015)
[50] Degasperis, A., Lombardo, S., Sommacal, M.: Rogue wave type solutions and spectra of coupled nonlinear Schrödinger equations, Fluids. MDPI (2019)
[51] Chen, S., Baronio, F., Soto-Crespo, J.M., Grelu, P., Mihalache, D.: Versatile rogue waves in scalar, vector, and multidimensional nonlinear systems. J. Phys A Math. Theor. **50**, 78 (2017)

Marzia Romano
Department of Mechanics, Mathematics and Management
Politecnico di Bari
70125 Bari
Italy
e-mail: marzia.romano@poliba.it

Sara Lombardo
Maxwell Institute for Mathematical Sciences
The Bayes Centre
Edinburgh
UK
e-mail: s.lombardo@hw.ac.uk

Sara Lombardo
Department of Mathematics
School of Mathematical and Computer Sciences (MACS) Heriot-Watt University
Edinburgh
UK

Marzia Romano and Matteo Sommacal
Department of Mathematics, Physics and Electrical Engineering
Northumbria University
Newcastle upon Tyne
UK
e-mail: matteo.sommacal@northumbria.ac.uk

(Received: July 27, 2022; revised: June 15, 2023; accepted: July 5, 2023)